Wireless Ceramic Sensors Operating in High Temperature Environments

Edward D. Birdsell
School of Mechanical Engineering, Georgia Institute of Technology, Atlanta, GA, 30332-0250

Jin-Woo Park
School of Electrical and Computer Engineering, Georgia Institute of Technology, Atlanta, GA, 30332-0250

Mark G. Allen
School of Electrical and Computer Engineering, Georgia Institute of Technology, Atlanta, GA, 30332-0250

A platform for the wireless transmission of data at high temperature is presented. The platform is demonstrated by means of a wireless temperature sensor fabricated from multilayer high-temperature ceramic MEMS technology. Extensions of the platform to chemical sensing are also discussed. As a first example of high temperature, wireless chemical sensing, a carbon dioxide sensor is implemented.

I. Introduction

In high-temperature environments, such as internal combustion and turbine engines, there exists a number of sensing applications. Pressure, temperature, and chemical specie concentration are all parameters of interest. In aircraft engines, sensors may be exposed to temperatures in the range of 600 to 1800°C. Development of sensors capable of operating under such extreme conditions presents a difficult materials related challenge.

Previous work has demonstrated that ceramic packaging techniques adapted from the microelectronics industry offer a material set well suited for operation in high-temperature environments. Utilizing multilayer ceramic laminate technology, sensors constructed from low-temperature co-fireable ceramic (LTCC) have been demonstrated. In particular, a wireless pressure sensor that can operate at temperatures up to 450°C[1]. The sensor, using LTCC, consists of a screen-printed planar spiral inductor connected in series to a pressure sensitive parallel-plate capacitor. This forms a passive LC circuit allowing wireless data retrieval using an external loop antenna. The passive nature of its operation removes the need for on-board power supplies, electronics, or exterior connections, thus eliminating their temperature limitations. The resulting sensor is well suited for use in high temperature environments

The temperature limitations that arise in devices fabricated using LTCC, originate from the glass component of the material. LTCC is a flexible ceramic green tape formed from a mixture of glass frit, ceramic powder, and organic binders. When cured, by heating, the glass component melts to bond the ceramic powder and becomes rigid upon cooling. This offers the advantage of a lower curing temperature than normally required for a pure ceramic composition. However, the glass component exhibits significantly higher conductivity than the ceramic at high temperature.

In this work, a temperature sensor for use in environments exceeding 800°C is fabricated using multilayer lamination of pure alumina ceramic (Al_2O_3) tape. A passive wireless resonant telemetry scheme, which has been previously demonstrated with the LTCC pressure sensor[2], is employed to measure temperature. Temperature variations are translated into frequency shifts that are remotely measured. A refined design of the temperature sensing platform is also demonstrated to have a potential application for wireless measurement of chemical species at high temperatures, by introduction of chemically-sensitive high temperature materials into the sensing platform.

II. Design and Fabrication – Temperature Sensors

The operation of the temperature sensor is based on the temperature-dependent nature of electrical properties in materials. The variable conductivity of metals and the semi-conducting behavior of ceramics are familiar concepts and used in a multitude of applications today. Ceramic materials are of particular interest for use in high temperature

sensors due to their electrical insulating properties that often remain, even at elevated temperatures. This makes ceramics an ideal candidate for use as a high temperature dielectric material. As may be expected, ceramics, in addition to conductivity, also exhibit a temperature related change in dielectric constant[3]. Fig. 1 demonstrates this effect of temperature on the dielectric constant of alumina (Al_2O_3).

The temperature dependent conductivity and permittivity of ceramics presents a straightforward sensing scheme involving a LC resonator circuit that has a resonant, f_o. Utilizing a temperature sensitive dielectric in the fabrication of the capacitor, results in temperature dependent capacitance values. The sensor exhibits a temperature dependent shift in resonant frequency.

A cross sectional schematic of the initial wireless temperature sensor, based on this LC circuit, is shown in Fig. 2. The sensor consists of three dielectric layers; one thin layer sandwiched between two thicker layers of similar material. Electrodes on either side of the thin dielectric form a parallel plate capacitor that is connected to a spiral inductor. The thick outer layers of dielectric protect the embedded circuitry and offer mechanical support; they serve no electronic function.

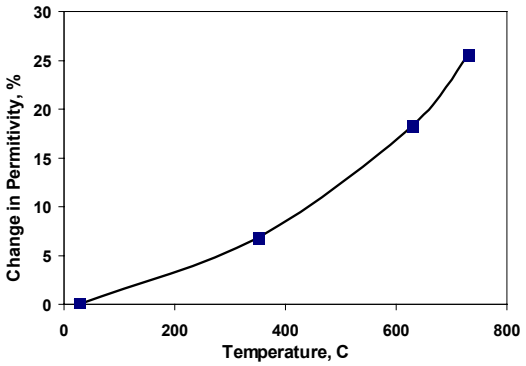

Figure 1. Change in permitivity of Al_2O_3 vs. temperature. Measured at a frequency of 40MHz

A modified wireless temperature sensor utilizes the identical principle, of temperature-dependant permittivity, as the previous sensor. However, a capacitor with interdigitated electrodes replaces the prior parallel plate configuration (Figs. 4, 5). This layout creates an exposed planar capacitor that enables post-processing addition of the dielectric material, as will be discussed later. As with the prior temperature sensor, temperature induced changes in the permittivity of the dielectric material result in f_o shifts. Fabrication procedures for the two temperature sensors are outline below.

A. Parallel-Plate Capacitor Temperature Sensor Fabrication

The body of the sensor is fabricated from high-purity (99.6%) sheets of alumina ceramic green-tape. This product is commercially available from multiple sources and is available in sheet thicknesses ranging from 25um to over 1000um. The green-tape is a mixture of alumina powder and organic binders that create a pliable sheet that is easily handled and machined. The organic binder system, a proprietary formulation of the vendor utilized[4], has been designed for lamination applications to improve adhesion between layers.

The bulk sheets of ceramic green tape are cut to size using a high power Nd:YLF laser. The energy of the laser beam is predominately absorbed by the organic binders in the green-tape. This absorption superheats and vaporizes the binders in a process referred to as ablation. Once vaporized, the binder material is jettisoned from the cut region carrying with it the ceramic particles. The laser used is a Resonetics Impressario micromachining system based around a 1047nm Nd:YLF laser operating at 1kHz with an output of 15watts at the cutting head. The laser beam is focused to a spot size of approximately 75µm and, if needed, can be reduced further with the use of apertures. The computer controlled x-y table, used for part positioning, is capable of an accuracy of ±0.1µm through the use of optical encoders. This accuracy combined with the small beam diameter enables more than sufficient dimensional control of the green-tape cutting.

Three layers of alumina ceramic green-tape are used in the construction of the sensor. Two 50mmx50mm squares of 0.5mm thickness and one 50mmx50mm square of 0.125mm thickness are cut using the laser system described above. A series of small 2mm diameter holes that aid in alignment are also cut in the sheets.

The two 0.5mm thick squares are each screen printed with a conductive ink pattern of an inductive coil and capacitor plate. The ink used is a commercially available composition of platinum (Dupont 9141) that incorporates a glass frit to aid in adhesion to Al_2O_3. After printing, the ink is baked in an oven at 100°C for one hour to drive off volatile solvents. This drying process is necessary to prevent the flow of ink during the lamination step.

Once the ink is dry, the three green-tape squares are aligned and stacked on aluminum platens. The 0.125mm thick layer is sandwiched between the two conductive surfaces of the 0.5mm thick layers. The assembly is next placed into a heated press (Carver Model C-26000). A pressure of 5.5MPa is applied to the sensor at a temperature of 75°C for 60 seconds to laminate the layers together.

After lamination, the sensor receives a two step heat treatment. It is first heated to 400°C at a rate of 3°Cmin-1. The slow heating rate is required to ensure that pressure within the sensor, due to the gas generated during organic binder burn-off, does not reach a level that will delaminates the layers. Once the sensor reaches 400°C, it is heated to the final sintering temperature of 1400°C at a rate of $5°C \cdot min^{-1}$. It is held at 1400°C for four hours to complete the sintering process where the ceramic particles bond and densify. The device is then cooled at $10°C \cdot min^{-1}$ to room temperature. The final device is a monolithic unit with an embedded platinum LC circuit. SEM analysis of sensor cross-section indicates that there are no distinguishable interfaces between the ceramic layers. Fig. 3 shows an example of a fabricated sensor. The embedded inductor coil and capacitor electrodes are visible with the use of backlighting.

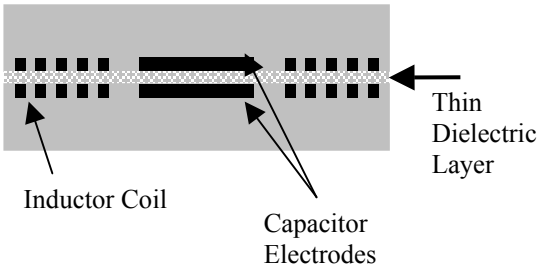

Figure 2. Cross section schematic of laminated temperature sensor.

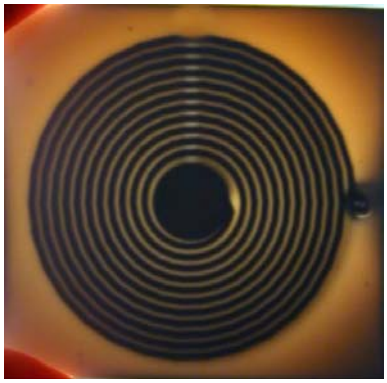

Figure 3. Example of fabricated sensor. Backlighting highlights embedded conductive coils and electrodes.

B. Interdigitated Capacitor Temperature Sensor Fabrication

The body of the sensor is fabricated from a high-purity alumina (99.6%) thin-film substrate obtained from Coors Ceramics Company (Superstrate 996). These substrates are 50.8mmx50.8mmx0.66mm in dimension and have an "as-fired" surface finish (non-polished). The fabrication sequence does not utilize alignment holes so machining of green tape is not required in this case.

The first step in fabrication is formation of the inductive coil. A seed layer of 200Å titanium and 2000Å copper is deposited with a DC sputter on the alumina substrate. On top of the seed layer a 10µm thick layer of negative photoresist (Futurexx NR9-8000P) is deposited. The photoresist is exposed and developed to form the electroplating mold for nickel. 10µm of Nickel is next electroplated using a Nickel Sulfamate bath at a current density of $5\ mA \cdot cm^{-2}$. Deposition rate was measured at $0.32\mu m \cdot min^{-1}$. After electroplating is complete, a passivation layer of 200Å titanium and 1000Å platinum is sputter deposited. This passivation layer serves as an oxidation barrier of the nickel to oxidation at elevated temperature. Following the passivation layer deposition, the photoresist mold is stripped and the exposed portions of the seed layer are removed using a standard etch.

The second fabrication step is construction of the interdigitated capacitor electrodes. This begins with stencil printing an 8mmx20mm rectangle of platinum ink 20µm thick. This is the same Dupont ink (9141) discussed earlier in the paper. The ink is dried at 100°C for six hours to completely drive off volatile solvents. Once dry the interdigitated electrodes of the capacitor are patterned into the ink using laser ablation. This process utilizes a 248nm excimer laser micromachining system (Resonetics MicroMaster/Lambda Physik LPX200). This laser micromachining system has a rated power of $600mJ \cdot pulse^{-1}$ and can operate at a frequency of 100Hz. The x-y part positioning table is computer controlled and, through the use of optical encoders, has a rated positioning accuracy of 0.1µm. The laser beam is rectangular in shape and has dimensions of 10mmx15mm. This beam can be masked,

using metal stencils, to project a beam of any shape or size needed in the machining process. Each material exhibits an ablation threshold of beam energy density, or fluence. Below this threshold the beam energy is absorbed by the material and only results in localized heating. No material will be removed. In the case of platinum ink, which contains organic binders, this threshold is well below that of sintered alumina. This enables the complete removal of the platinum ink without concern for damage to the underlying ceramic substrate.

To create the interdigitated electrode pattern the beam is shaped using a stainless steel stencil mask with a 500µmx500µm square opening. This imaged beam undergoes a 4.5X demagnification resulting in an approximate 110µmx110µm square beam at the sample position. The beam energy is attenuated to a fluence of 0.95 $J \cdot cm^{-2}$ which, as noted before, is well below the ablation threshold of the alumina substrate. A preprogrammed computer controlled pattern defining the electrodes is cut into the deposited layer of platinum ink. This process creates a well defined and uniform 110µm gap between the capacitor electrodes. Once the electrodes are defined, the ink is cured to remove the remaining binders and densify the platinum powder and frit. The sensor is placed in a furnace (Lindberg model BF51848) and heated to 1000°C, in an air atmosphere, at a ramp rate of $10°C \cdot min^{-1}$ and held for 30 minutes before cooling to room temperature at a rate of $10°C \cdot min^{-1}$. Fig. 4 below shows this completed sensor. Fig. 5 is a magnified view of the interdigitated capacitor after the electrodes are patterned into the platinum ink.

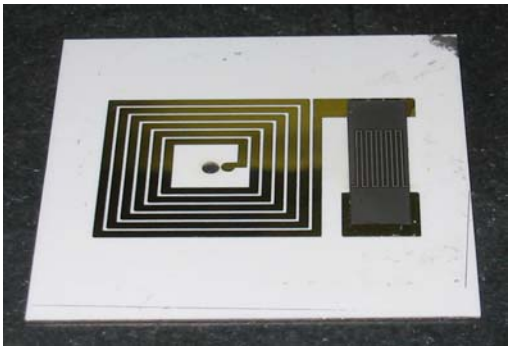

Figure 4. Temperature sensor. Electroplated inductive coil with screen printed, laser machined interdigitated capacitor. Note laser machined via in center of coil for completion of the LC circuit.

Figure 5. Magnified view of interdigitated capacitor. Screen printed platinum capacitor with laser machined electrodes. Electrode gap is 110µm.

III. Chemical Sensor Design and Fabrication

At high temperature, chemical sensing predominately involves a potentiometric approach using solid electrolytes. For most straightforward extension of the current wireless sensing platform, however, an approach involving materials exhibiting dielectric constant and resistance change with chemical species was investigated. Capacitive detection schemes presented for gas measurement have been generally limited to low-temperature applications (e.g. humidity, hydrocarbon sensors[5]). However, work by Ishihara[6-8], has shown that certain mixed oxide compositions containing $BaTiO_3$ demonstrate a high-temperature dielectric response to CO_2 exposure. One such composition is an equal molar mixture of $BaTiO_3$-La_2O_3. It is reported to exhibit measurable permittivity changes over a CO_2 concentration range of 100ppm-80,000ppm[7]. This change in dielectric constant is believed to result from a carbonation of the La_2O_3 by CO_2[7, 8]. Producing a measurable response requires that the material is exposed to CO_2 at a temperature above the decomposition point of the carbonate. Temperature elevations above this point increase sensitivity until it reaches maximum sensitivity at 766°C[7]. Although such thermal requirements may be unsuitable for typical sensors, they are particularly attractive for high temperature sensing applications.

One approach to developing a passive chemical sensor is to incorporate a material with a chemically sensitive dielectric constant similar that discussed above. The design of the temperature sensor is well suited to incorporating such materials. Deposition of sensing material directly on to the interdigitated capacitor leaves one side completely exposed to the environment, eliminating the need for porous electrodes and simplifying fabrication.

Electrical modeling of the sensor shows that there are two distinct approaches to generating a measurable change in the impedance of the loop antenna. One approach, as used in the temperature sensor, is to vary the capacitance of the sensor circuit. The alternative approach is to vary the conductivity of the dielectric material. Instead of producing

resonant frequency shifts, changes in conductivity create variations in the magnitude of the measured impedance angle at the f_o of the sensor. The fabrication process, of one such CO sensor, follows.

A. Chemically Sensitive Dielectric Material Preparation

A chemically sensitive dielectric material of equal molar $BaTiO_3$-La_2O_3 is prepared using traditional powder processing techniques[9]. The beginning materials are commercially available powders of high purity, fine grained $BaTiO_3$ and La_2O_3. First, appropriate quantities of each component necessary to prepare a 1:1 mole ratio of powder are measured. The target batch size of the mixture is 5g-10g.

The measured batch is next mixed by ball milling. The batch is placed into a 250mL wide-mouthed Nalgene® bottle. Cylindrical alumina grinding media, 12.7mm diameter x 12.7mm length, are added to the bottle. The required amount of media, approximately 50 units, fills one-half of the bottle volume. Next, the bottle is filled with a sufficient volume of DI water to entirely cover the grinding media (approximately 200mL). The bottle is then sealed and placed on a roller mill and turned at 60rpm for 24 hours. This milling process serves to breakup any powder conglomerates, mix the components, and reduce the overall grain size of the material. The resulting mixture is highly uniform in particle size and composition. After the batch has milled for 24 hours, the liquid suspension of powder is poured into a 20mmx150mm Pyrex® Petri dish. The suspension is then heated to 90°C for 12 hours to completely drive off the water.

Once dry, the powder is made into a printable ink. The powder is combined with glycerin and mixed using a mortar and pestle. A weight ratio for glycerin to powder of 0.1:1 produces an ink with an acceptable consistency and viscosity for screen or stencil printing. Glycerin decomposes above 290°C and is easily removed during heat treatment.

B. CO_2 Gas Sensor Fabrication

The chemical sensor fabrication follows the identical process as that used for the temperature sensor with an interdigitated capacitor. However, one additional fabrication step is added at the end of the process to deposit the chemically sensitive dielectric. The previous prepared dielectric ink is stencil printed, using a rectangular 10mmx14mm stencil, on to the surface of the capacitor electrodes. The sensor is then heated at a rate of $3°C \cdot min^{-1}$ to 630°C and held for a duration of 5 hours prior to cooling to room temperature at $10°C \cdot min^{-1}$. The heating burns off the glycerin and the 5 hour dwell time calcines the $BaTiO_3$-La_2O_3 mixture. An insignificant amount of sintering occurs during the calcining and the resulting mixture remains porous upon cooling to room temperature. Previous x-ray diffraction work with this material indicates that it remains a simple mixture of separate $BaTiO_3$ and La_2O_3 particles[6].

IV. Modeling

The equivalent electrical circuit model of the ceramic temperature sensor, with a coupled measurement antenna, is illustrated in Fig. 6. L_a, L_s, and L_m refer to the antenna inductance, sensor coil inductance, and the mutual inductance, respectively. R_s is the series resistance of the inductive sensor coil and R_p is the parallel resistance, due to leakage, across the sensor capacitor, C_s. The input impedance, Z_a, of the antenna can be modeled from this circuit using Eqs. (1,2, and 3). The process for the derivation of Eq. 1 has been detailed in previous work[1].

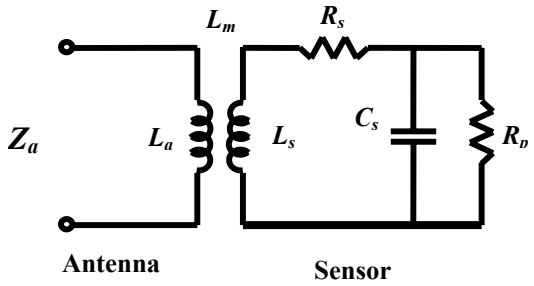

Figure 6. Equivalent electrical circuit of antenna and sensor.

$$Z_a = \left[\frac{\omega^2 k^2 L_s L_a A}{A^2 + B^2} + j\left(\omega L_a - \frac{\omega^2 k^2 L_s L_a B}{A^2 + B^2} \right) \right] \quad (1)$$

$$A = R_s + \frac{R_p}{1 + \omega^2 C_s{}^2 R_p{}^2} \quad (2)$$

$$B = \omega L_s - \frac{\omega C_s R_p{}^2}{1 + \omega^2 C_s{}^2 R_p{}^2} \quad (3)$$

$$k^2 = \frac{L_m^2}{L_a L_s} \quad (4)$$

In our experimental setup, phase of impedance, Z_a is measured. The coupling factor k, L_s, and L_a remain constant in the testing setup and do not contribute to changes in Z_a. However, variables R_s, R_p and C_s can shift. The measurement approach used by the temperature sensors employ this variation in C_s. Conversely, chemical sensor testing results, for geometries and materials tested to date, have indicated that R_p variations dominate the sensor response.

Design of the interdigitated capacitor, used in both the temperature and chemical sensor, is analyzed using finite element analysis. Figure 7 shows the geometrical dimensions of the sensor capacitor designed. The interdigitated capacitor has five fingers for each electrode. The two electrodes are separated by a uniform gap of 60μm. In order to predict the capacitance value of the interdigitated structure, analysis has been performed using ANSYS 7.1. The geometry used for two-dimensional electrostatic simulation is shown in Fig. 8. The capacitance without the chemically sensitive material is simulated first. With a relative permittivity of 10 for the ceramic substrate (typical permittivity of alumina is 9~11), the simulated capacitance is 5.39μF, which is 36% higher than the measured capacitance. The discrepancy between measured and calculated capacitances could be attributed to a slightly over-etched ceramic gap during laser ablation of the electrodes and the permittivity variation of the ceramic sample. The relative permittivity that best fits the measured capacitance is found to be 7. After applying chemically sensitive

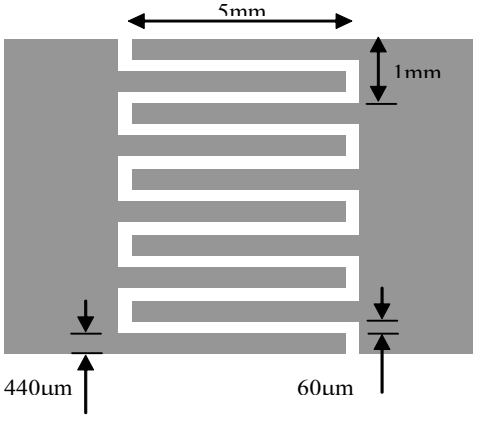

Figure 7. Geometry of sensor capacitor used in simulation (top view).

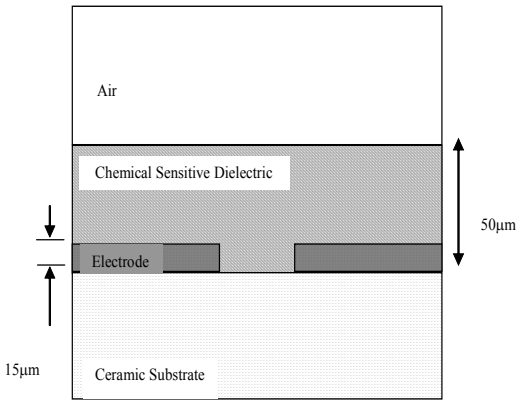

Figure 8. Capacitor geometry for 2D electrical analysis.

material, the capacitance has been measured to be 9.48μF. The relative permittivity of the sensor materials was calculated using simulation and the value is 18. Figure 9 shows the simulation result of electric displacement for the gap capacitance with the sensor material. These values of 7 and 18 can be used for modeling the effect of alternative geometries.

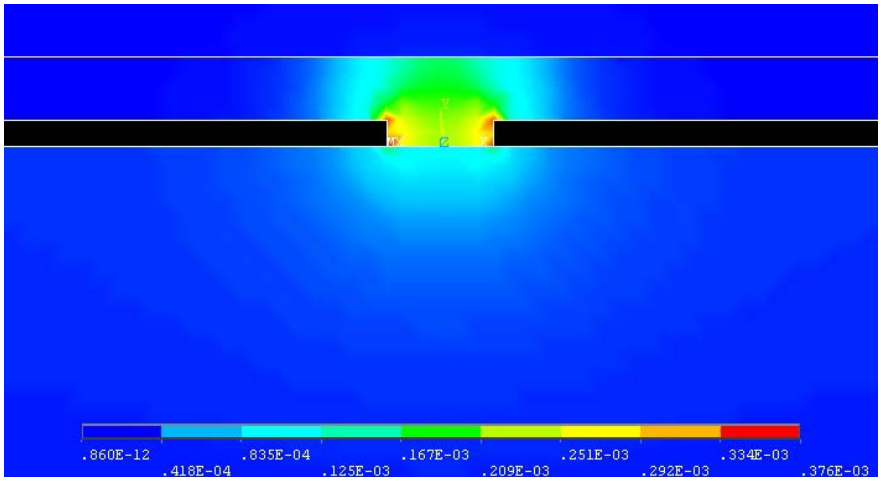

Figure 9. Simulated electric displacement of the gap capacitance with layer of chemically sensitive dielectric.

V. Testing

A. Temperature Sensor Testing

Measurements for the temperature sensors are conducted using a Lindberg box furnace (Model BF51848) that has a maximum temperature of 1100°C. The furnace is fitted with a feed-through to pass a loop antenna inside the heated chamber. An antenna is constructed from a 50cm length of 1mm diameter Nickel-Chromium wire. The sensor is placed within the plane of the antenna loop and the impedance *Z* of the antenna is measured as a function of frequency using a HP4194A impedance analyzer. The furnace is ramped to each measurement temperature point and allowed to equilibrate for 30 minutes before data is taken. A K-type thermocouple located directly adjacent to the sensor serves to monitor localized temperature and confirm accuracy. Results are shown below in figs. 10 and 11. Figures 10 and 11 display the measured phase angle in relation to frequency at various temperatures. There is a notable widening of the trough and decrease in peak phase angle magnitude as temperature increases indicating a reduction in quality factor, Q. This results from both the increased resistance of the inductive coil and increased conductivity of the insulating ceramic. The minimum phase angles shown in Figure 11 correspond to the resonant frequencies of the sensor. Figure 12 plots this change in resonant frequency with relation to temperature with the sensor exhibiting a sensitivity of -4.53kHz·C^{o-1}.

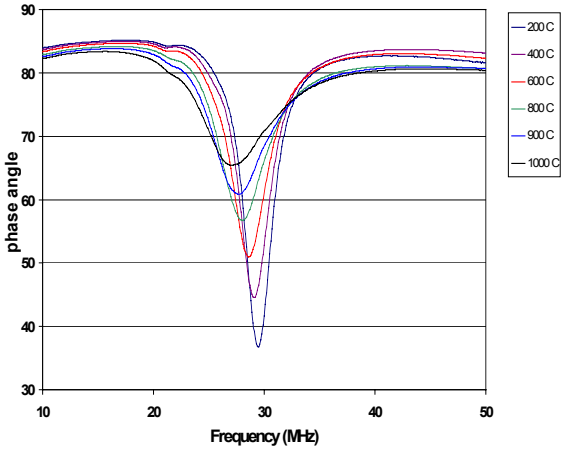

Figure 10. Impedance phase angle vs. frequency for temperature sensor.Parallel plate design.

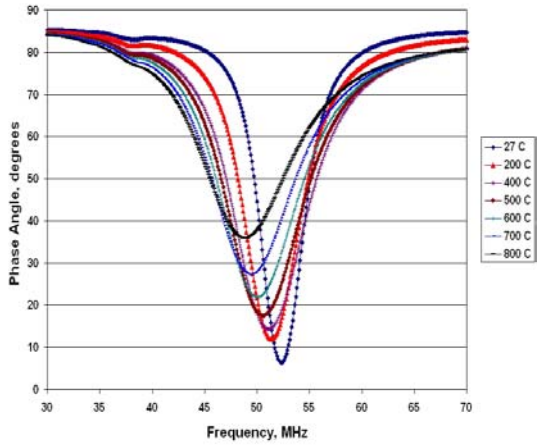

Figure 11. Impedance phase angle vs. frequency for temperature sensor. Interdigitated capacitor design.

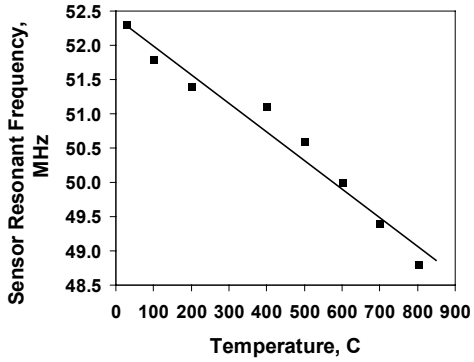

Figure 12. Resonant frequency vs. temperature. Temperature Sensor.

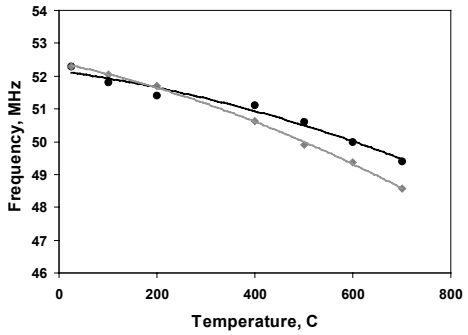

Figure 13. Resonant frequency vs. temperature for sensor. Comparison of measured and predicted values.

B. $BaTiO_3$-La_2O_3 Characterization

To accommodate fabrication and testing constraints, the optimum resonant frequency design range for these high temperature sensors is 20-60 MHz. Dielectric properties reported in the literature are typically from measurements taken within a frequency range of 50kHz-1MHz. This presents a need for further material characterization of the potential materials. Figure 14 illustrates the frequency dependent sensitivity of $BaTiO_3$-La_2O_3 when exposed to a gas mixture of 50:50 CO_2 and dry air. There is a significant falloff in sensitivity at higher frequencies. Below 1MHz, $BaTiO_3$-La_2O_3 exhibits a change in permittivity approaching 10%. However, above 20 MHz, the response falls to 1-2%. This behavior is an important consideration in sensor design.

As discussed earlier, an alternative approach to chemical detection in these sensors is to utilize chemically dependent variations in the conductivity of the dielectric material. In the case of $BaTiO_3$-La_2O_3, in addition to exhibiting a CO_2 concentration dependent permittivity, it also exhibits a CO_2 concentration dependent resistivity. Figure 15 demonstrates the effect of CO_2 exposure to the DC conductivity of $BaTiO_3$-La_2O_3. A response up to a 6.5% increase in resistivity is generated with exposure to pure CO_2.

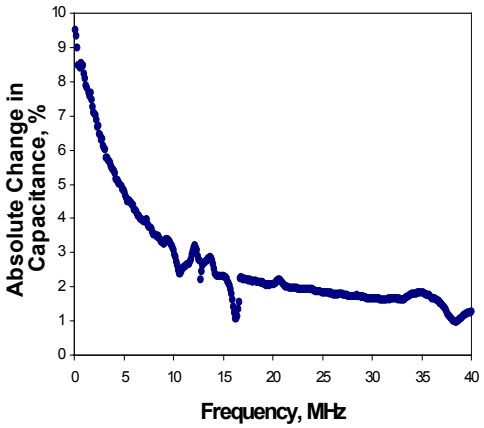

Figure 14. Frequency dependence sensitivity of $BaTiO_3$-La_2O_3. Sample exposed to 50:50 mixture of CO_2-Dry Air. Note that actual change in capacitance is

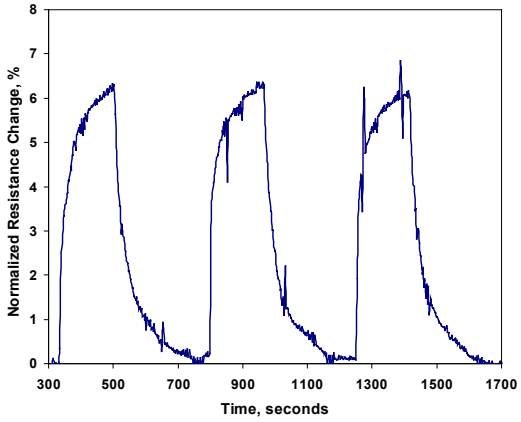

Figure 15. Normalized resistance change vs. time for $BaTiO_3$-La_2O_3 exposed to 100% CO_2.

C. CO_2 Gas Sensor Testing

The experimental setup for CO_2 gas sensor uses the same furnace and loop antenna arrangement constructed for the temperature sensor measurements. In order to control the atmosphere within the furnace, a 1mm I.D. stainless tube is inserted into the furnace floor. This tube is connected to the output of two Aalborg gas flow meters that are used to mix incoming air. The meters are supplied with ultra-pure dry air and analytical grade CO_2 from compressed gas cylinders. The furnace is supplied with a constant flow of dry air at a rate of 163 $smL \cdot min^{-1}$. This flow is sufficient to create a positive pressure within the furnace and allow control of atmospheric conditions within the chamber. As before, the sensor is placed in the plane of the loop antenna. The sample is heated at a rate of $5° \cdot Cmin^{-1}$ to 670°C and allowed to stabilize for 6 hours. After stabilization measurements are taken to establish the sensor baseline. Various known volumes of CO_2 are mixed with the constant supply of dry air entering the test chamber. Each concentration of CO_2 is exposed to the sensor for a period of 5 minutes prior to measurement. After exposure and measurement, the flow of CO_2 is stopped and the dry air is allowed to purge the chamber for 30 minutes. Response of the sensor is measured at CO_2 concentrations of 10, 37, and 100% and the results are shown in Fig. 16. Figure 16 shows the a measurable decrease in the impedance phase angle that is proportional to the CO_2 concentration. Previous measurements of the $BaTiO_3$-La_2O_3 indicate that exposure to CO_2 increases the resistance of the material (Fig. 15). According to the electrical model presented earlier, this increase in dielectric resistance should result in a decrease in phase angle, as is demonstrated here. Incorporating actual measured changes of conductivity into our model, we are able to calculate the predicted change in phase angle. Comparison between

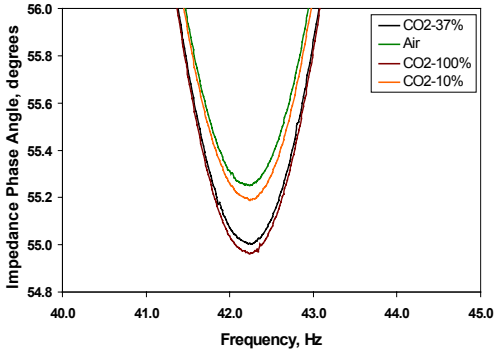

Figure 16. Impedance phase angle vs. frequency. Sensor exposed to differing CO_2 concentration.

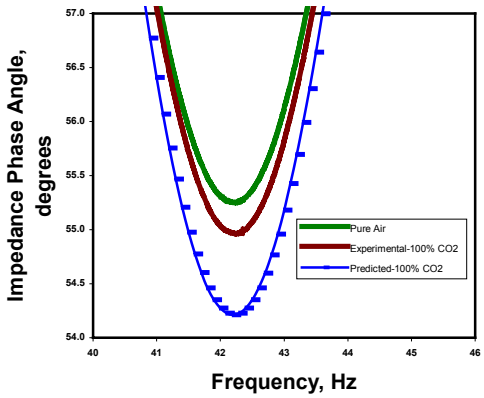

Figure 17. Impedance phase angle vs. frequency. Predicted and experimental comparison.

predicted and experimental data is shown in Fig. 17. At 100% CO_2, the simulation predicts an approximate 1.0° in phase angle. However, experimental data produces a 0.3° decrease. One potential explanation for this discrepancy is that the conductivity data were DC measurements. As in the case of dielectric permittivity, electrical conductivity of the $BaTiO_3$-La_2O_3 may also exhibit a frequency dependence.

VI. Discussion and Conclusion

The temperature sensor demonstrates a platform capable of wireless transmission of data at temperatures exceeding 800°C. Additionally, the performance of the sensor correlates well to design and modeling predictions. Utilization of an interdigitated surface-machined capacitor enables straightforward adaptation of this platform to a chemically sensitive sensor. Preliminary investigation has identified $BaTiO_3$-La_2O_3 as one potential material that demonstrates a dielectric response to CO_2 at elevated temperature in the frequency regime of interest.

Acknowledgments

This work was supported in part by the National Aeronautics and Space Administration (NASA) University Research, Engineering and Technology Institutes (URETI) program in the area of aeropropulsion. The authors would like to thank Mr. Richard Shafer of Georgia Tech for valuable technical assistance.

References

[1]Fonseca, M. A., English, J. M., von Arx, M., Allen, M. G., "Wireless Micromachined Ceramic Pressure Sensor for High-Temperature Applications," *Journal of Microelectromechanical Systems*, Vol. 11, No.4, Aug. 2002.

[2]English, J. M., Allen, M. G., "Wireless Micromachined Ceramic Pressure Sensors," *Proceedings IEEE MEMS '99*, 1999, pp. 511-516.

[3]Hench, L., and West, J., Principles of Electronic Ceramics, John Wiley and Sons, New York, 1990, Chaps. 5,6.

[4]Richard E. Mistler, Inc., Morrisville, PA, 19067, USA

[5]Ishihara, T., Matsubara, S., "Capacitive Type Gas Sensors," *Journal of Electroceramics*, Vol. 2, No. 4, 1998, pp. 215-228.

[6]Ishihara, T., Kometani, K., Mizuhara, Y., Takita, Y., "Mixed Oxide Capacitor of CuO-BaTiOc as a New Type of CO2 Gas Sensor," *Journal of the American Ceramic Society*, Vol. 75, No. 3, 1992, pp. 613-618.

[7]Ishihara, T., Kometani, K., Hashida, M., Takita, Y., "Application of Mixed Oxide Capacitor to the Selective Carbon Dioxide Sensor," *Journal Electrochemical Society*, Vol. 138, No. 1, Jan. 1991.

[8]Ishihara, T., Kometani, K., Mizuhara, Y., Takita, Y., "Capacitive-Type Gas Sensor for the Selective Detection of Carbon Dioxide," *Sensors and Actuators B*, Vol. 13-14, 1993, pp. 470-472.

[9]Reed, J., Introduction to the Principles of Ceramic Processing, John Wiley and Sons, New York, 1988, Chap. 16.